SolarPACES Conference 2023

Thermal Energy Storage Materials, Media, and Systems

https://doi.or/10..... DOI placeholder (WILL BE FILLED IN BY TIB Open Publishing)

Published: (WILL BE FILLED IN BY TIB Open Publishing)

Performance Evaluation of a 40-kW$_{th}$ Prototype Counterflow Particle-sCO$_2$ Fluidized Bed Heat Exchanger

Winfred J. Arthur-Arhin[1][https://orcid.org/0000-0003-2045-1733], Jesse R. Fosheim[4][https://orcid.org/0000-0001-7794-3558], Keaton J. Brewster[1][https://orcid.org/0000-0002-3307-3228], Kevin J. Albrecht[2,3], Dimitri Madden[3][https://orcid.org/0009-0001-4086-3922], and Gregory S. Jackson[1] [https://orcid.org/0000-0002-8928-2459]

[1] Colorado School of Mines, Golden, CO
[3] Sandia National Laboratories, Albuquerque, NM
[3] Vacuum Process Engineering, Inc. Sacramento, CA
[4] Brayton Energy LLC, Hampton, NH

Abstract. Particle-sCO$_2$ heat exchangers (HXs) can couple particle-based thermal energy storage for concentrating solar power (CSP) plants with recompression closed Brayton power cycles (RCBC) to enable continuous dispatchable renewable electricity. RCBC firing temperatures >700°C require HXs with expensive Ni-based alloys, requiring HX designs to reduce mass with high overall heat transfer coefficients U_{HX} to meet CSP primary HX cost. To enhance U_{HX}, mild bubbling fluidization with downward particle flows and upward fluidizing gas flows can achieve particle-wall heat transfer coefficients $h_{T,w}$ >800 W m^{-2} K^{-1} with CARBOBEAD HSP 40/70. To assess how high $h_{T,w}$ with mild particle fluidization impacts U_{HX}, a 40-kW$_{th}$ particle-sCO$_2$ HX with 12-parallel narrow-channel fluidized beds was assembled and tested to particle inlet temperatures up to 530 °C. Tests show reliable steady-state HX operation by maintaining fluidized particles in a freeboard zone above the parallel channels, but axial dispersion mixes partially cooled particles up from the fluidized channels with particles fed into the freeboard zone from the feed hopper. This mixing lowers the effective bed temperatures and the driving force for heat transfer to counterflowing sCO$_2$ in microchannelled walls. Measured U_{HX} based on particle inlet temperature never exceeded 205 W m^{-2} K^{-1}. The trade-off between increased $h_{T,w,}$ and increased vertical dispersion with gas flows resulted in only small improvements in U_{HX} after the onset of fluidization. Dispersion was incorporated into HX design and performance models that used $h_{T,w}$ correlations fitted to single-channel heat transfer tests. Model results show that reducing dispersion leads to higher particle wall heat transfer.

Keywords: Concentrating Solar Power, Particle Heat Exchangers, Fluidized Bed Heat Transfer

1. Introduction

With high densities ($\rho_s \geq$ 2500 kg m^{-3}), high specific heats ($c_{p,s}$ ≈ 1200 J kg^{-1} K^{-1} at 600 °C), mechanical robustness, and low costs on the order of $1 kg^{-1}, inert oxide particles such as silica sand or Carbo Ceramics HSP can provide an attractive thermal energy storage (TES) and heat transfer media for TES above 600°C [1] in concentrating solar power (CSP) plants [2]. Oxide particles can couple to efficient recompression closed Brayton power (RCBC) cycles that use

supercritical carbon dioxide (sCO_2) with a particle-sCO_2 heat exchanger (HX) that supplies sCO_2 turbine inlet temperatures above 700 °C [3]. To meet US Department of Energy (DOE) cost targets of $\leq$ \$15/kWh$_{th}$ for TES subsystems [2], particle-sCO_2 HX must achieve overall heat transfer coefficients U_{HX} approaching 600 W m^{-2} K^{-1} at high temperatures to reduce the required mass of expensive Ni alloys according to an analysis by Sandia National Laboratories (Sandia) of shell-and-plate, moving-packed-bed, particle-sCO_2 HXs [4]. Sandia demonstrated a 20-kW$_{th}$ moving-packed bed HX with the highest U_{HX} approaching 400 W m^{-2} K^{-1} with 3 mm deep particle-bed channels operating at off-design conditions [4]. Alternative approaches to achieve higher U_{HX} require lowering the limiting thermal resistance of particle-wall heat transfer in particle-sCO_2 HXs.

Fluidized bed HXs have been identified as an alternative approach to improve overall U_{HX} by lowering the particle-wall thermal resistance at similar conditions [5]. Flowing particles in narrow channel beds under relatively mild bubbling fluidization with upward gas flow can achieve particle-wall heat transfer coefficients $\approx 4\times$ larger than non-fluidized, particle flows [7,8]. However, parasitic loads and operational complexities associated with supplying the fluidizing gas flows raise questions regarding the pathway to meet cost-driven performance targets. On the other hand, the ability to achieve higher heat transfer at very low gas-to-particle mass flow ratios, $\dot{m}_g/\dot{m}_s < 2.0\%$, suggests that parasitic energy losses may be kept small. Lab-scale testing in single-channel fluidized beds at HX conditions led to a correlation for the particle wall heat transfer coefficient $h_{T,w}$ as a function of fluidization gas velocities following the approach of Molerus [8,9]. The fluidized-bed heat transfer correlations were implemented in a reduced-order particle-sCO_2 HX model to explore how HX geometry and operating conditions impact performance.

The reduced order HX model was used to identify preferred design and operating conditions for a demonstration particle-sCO_2 HX to achieve 40-kW$_{th}$ heat transfer in a shell-and-plate fluidized bed HX design. The 40 kW$_{th}$ thermal duty was predicted at a particle and sCO_2 flow rates $\dot{m}_s$ = $\dot{m}_{sCO2}$ = 0.2 kg s^{-1} with inlet temperatures $T_{s,in}$ = 600ºC and $T_{sCO2,in}$ = 400ºC [5]. Using CARBOBEAD HSP particles (mean diameter, d_p = 360 μm), the prototype HX model predicted overall $U_{HX} \approx$ 500 W m^{-2} K^{-1} at an HX effectiveness $\varepsilon = 0.81$. To evaluate the feasibility of the model-derived fluidized bed HX design for TES applications, a 40-kW$_{th}$ fluidized bed particle-sCO_2 HX with 12 parallel narrow-channel fluidized beds and microchannels for sCO_2 flows embedded in the bed confining walls has been fabricated from stainless steel in collaboration with Vacuum Process Engineering (VPE). The HX has been tested at Sandia's National Solar Thermal Test Facility (NSTTF) with the experimental setup explained in detail by Arthur-Arhin et al. (2023) [6]. Heat exchanger test results, as presented here, did not achieve the predicted performance due to axial dispersion in the narrow-channel fluidized bed causing undesirable vertical mixing and loss of temperature driving force to drive heat transfer. The HX tests did show that the parallel narrow-channel fluidized beds can operate reliably with a common freeboard zone, but only at an overall U_{HX} just above 200 W m^{-2} K^{-1} due to vertical mixing, and these results as discussed below, show the importance of employing approaches to reduce axial dispersion in the fluidized bed to take full advantage of the increased particle-wall heat transfer rates.

2. Heat Exchanger Design and Test Facility

The demonstration fluidized-bed particle-sCO_2 HX has been fabricated by VPE by diffusion bonding 304 stainless steel plates with embedded (etched) microchannels for internal sCO_2 flows and spacers between walls to frame the fluidized bed channels. The HX core consisted of 12 parallel narrow particle-bed channels with a common freeboard zone above the fluidized bed channels into which particles are fed through a rotating scoop valve. The upward fluidizing gas flows are injected into each fluidized channel of downward flowing particles through injector tubes (6.35 mm outer diameter) which span the width of each channel near the bottom of the core. A

common air manifold feeds the 12 injector tubes staggered at 86 mm and 102 mm above the base of the HX core. Particles underneath the injectors in the channels are not fluidized leading to moving packed bed flow for about 17% of the total heat transfer area of the HX. The HX core had an overall height Δy_b = 0.588 m (of which the top 0.45 m was fluidized above the injectors), individual fluidized bed depths Δz_b = 10.5 mm, and overall fluidized bed channel width Δx_b = 0.2 m. The total particle-wall heat transfer area $A_{w,tot}$ = 2.63 m^2 for all of the fluidized beds combined provides a basis for calculating an overall U_{HX}.

For the HX tests, CARBO HSP particles entered the fluidized bed channels from a common freeboard zone above the core as shown in Fig 1. Particles were fed into the freeboard zone from a channel at the bottom of a wedge feed hopper with a rotating scoop valve as shown in detail in Fig. 1 regulating the inlet flow to maintain particle inventory in the core and for a few cm of height in the freeboard zone. The feed hopper takes preheated particles from a 60-kW electric heater installed at NSTTF. Additional height in the freeboard zone allowed for particle-gas separation such that the fluidizing gas could leave the heat exchanger without significant particle entrainment as suggested in Fig 1. The freeboard zone is above the sCO_2 outlet header, so there is no direct heat transfer to the sCO_2 in the freeboard zone. In the HX core, heat is transferred from the fluidized particles in the channels to sCO_2 moving upward through laser-etched microchannels.

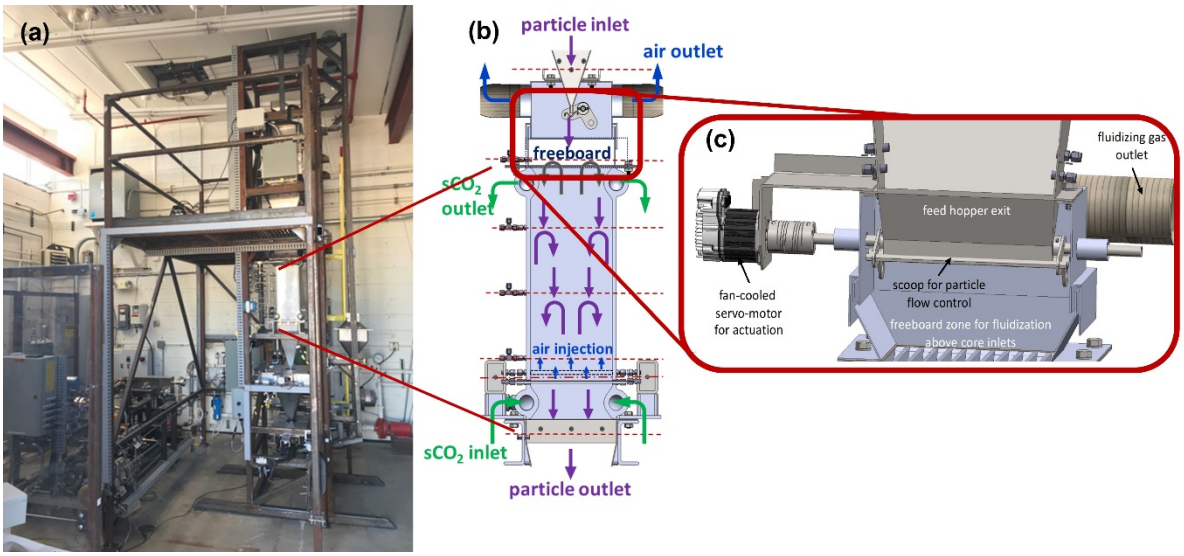

Figure 1. a) A picture of the heat exchanger assembly at the NSTTF b) Assembly drawing of 40-kWth fluidized-bed, particle-sCO2 heat exchanger core showing the flow of particles mixing and axial dispersion due to bubbling fluidization, with c) an exploded view of the cross-section of the freeboard zone.

Instrumentation in the HX provides pressure and bed temperature measurements at four different heights in four of the twelve channels and temperatures at multiple locations in the inlet hopper, freeboard zone, and outlet hopper. Pressure measurements in the bottom of the freeboard zone provided a basis for assessing whether the freeboard zone maintained adequate particle inventory for feeding the fluidized bed channels evenly. sCO_2 flows through the microchannels embedded in the walls were only measured at the inlet and outlet manifolds as shown in Fig. 1. Particle mass flow rates were measured in a weigh hopper beneath the outlet particle sliding-gate, flow-control valve at the bottom of the outlet hopper. The weigh hopper was intermittently emptied into a skip hoist which recycled particles to the top of the particle inlet heater at the top of the test facility.

The 40-kW_{th} stainless-steel fluidized bed HX tests at the NSTTF were conducted with CARBOBEAD HSP 40/70 (mean $d_p \approx 360$ μm) and HSP 45/60 (mean $d_p \approx 287$ μm) at particle inlet temperatures up to 530 °C, which was below the design conditions due to the need to protect the electric preheater from stagnant flow regions that could leave to overheating of the heating elements. The prototype HX test conditions listed in Table 1 did provide adequate results to calibrate the reduced-order model and thereby use it to understand performance at other HX operating conditions at higher *T* expected for CSP-TES applications.

Table 1. Stainless-steel fluidized bed particle-sCO_2 heat exchanger design flow conditions for testing at the National Solar Thermal Test Facility.

HX Flows	Property	Tested conditions	Design conditions
CARBOBEAD HSP particles	mean diam. d_p	287 μm / 360 μm	360 μm
	solid density ρ_s	3610 kg m^{-3}	3610 kg m^{-3}
	inlet temp., $T_{s,in}$	< 530 °C	600 °C
	mass flow rate, $\dot{m}_s$	< 200 g s^{-1}	200 g s^{-1}
fluidizing air	inlet temp., $T_{g,in}$	< 300 °C	400 °C
	mass flow rate, $\dot{m}_g$	< 5.0 g s^{-1}	2.0 to 4.0 g s^{-1}
supercritical CO_2	inlet temp., $T_{sCO2,in}$	200 °C	400 °C
	mass flow rate, $\dot{m}_{sCO2}$	200 g s^{-1}	200 g s^{-1}
	inlet pressure, $P_{sCO2,in}$	17 MPa	17 MPa

3. Heat Exchanger Results and Discussion

Numerous HX tests were performed at fixed particle and sCO_2 mass flow rates $\dot{m}_s$ and $\dot{m}_{sCO2}$ constant inlet temperatures $T_{s,in}$ and $T_{sCO2,in}$. For those fixed conditions, fluidizing gas mass flow rates $\dot{m}_g$ were varied to explore how HX performance changes with excess fluidization gas velocities as characterized by the dimensionless excess velocity $\widehat{U}$ defined in Eq. 1. and used in correlations for particle-wall $h_{T,w}$ [8,9].

$$\widehat{U} = \left(u_g - u_{mf}\right)\left(\rho_s c_{p,s}/\lambda_g g\right)^{1/3} \quad (1)$$

Where $u_g - u_{mf}$ represents the difference between the fluidizing gas velocity and the minimum fluidization velocity. The overall U_{HX} was expected to increase with $\widehat{U}$ up to values of 50 due to the expected rise in the $h_{T,w}$ with $\widehat{U}$ as predicted by Fosheim et al 2022 [8]. Figure 2 shows results for fluidized bed HX $\dot{Q}_f$ and U_{HX} calculated from Eq. 2 for a range of $\widehat{U}$ for $\dot{m}_s$ up to 0.25 kg s^{-1}.

$$\dot{Q}_f = U_{HX} A_{w,tot} \Delta T_{lm} = U_{HX} A_{w,tot} \frac{\left(T_{s,in} - T_{sCO2,out}\right) - \left(T_{s,out} - T_{sCO2,in}\right)}{\ln\left(T_{s,in} - T_{sCO2,out}\right) - \ln\left(T_{s,out} - T_{sCO2,in}\right)} \quad (2)$$

The results in Fig. 2a show that the fluidized bed HX provided the design target $\dot{Q}_f \approx 40$ kW_{th} to the sCO_2 flow only at the highest $\dot{m}_s \approx 0.25$ kg s^{-1} for $\widehat{U} \geq 10$. The higher $\dot{m}_s$ was required in part because the test inlet temperatures were below the design values and both $h_{T,w}$, and the heat transfer coefficient $h_{T,sCO2}$ to the sCO_2 microchannel flows increased with temperature [8]. Higher $\dot{Q}_f$ at the highest $\dot{m}_s$ is accompanied by slight increases in U_{HX} due to the increase in heat transfer coefficients with higher particle temperatures. U_{HX} increases substantially from its non-fluidized value $\widehat{U} < 0$ up to $\widehat{U} \approx 10$ showing the potential of fluidization to increase heat transfer. However, counter to expectations, U_{HX} does not increase with fluidization gas velocities for $\widehat{U} > 10$ despite the increase in particle-wall $h_{T,w}$ with $\widehat{U}$ served in the single-channel lab-scale tests [8].

Furthermore, for all the values of $\dot{m}_s$, the measured U_{HX} values based on particle inlet temperature $T_{s,in}$ from the feed hopper as indicated in Eq. 2 were below the U_{HX} predicted with the reduced order model with the highest $U_{HX} \approx 205$ W m^{-2} K^{-1} at a $\widehat{U} \approx 10$ and $\dot{m}_s = 0.25$ kg s^{-1}.

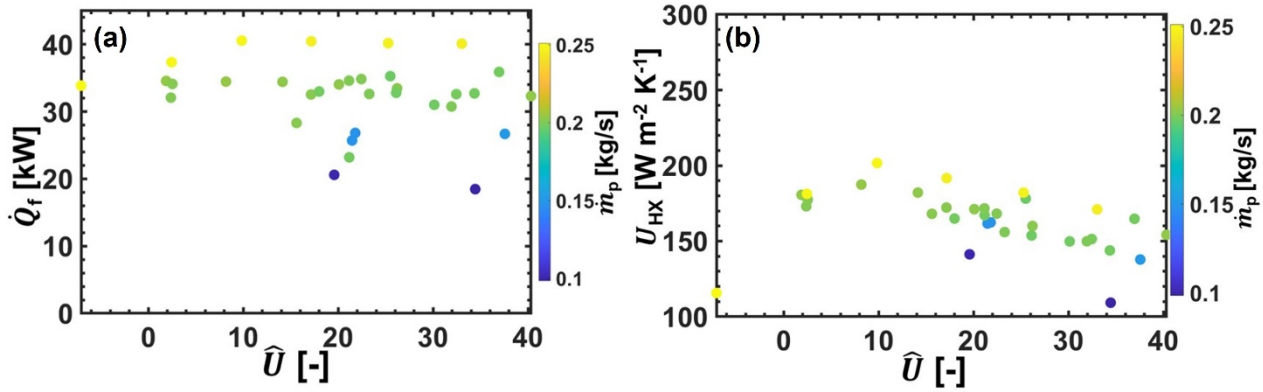

Figure 2. Experimental measurements of the particle flow rate $\dot{m}_s$ as colored points showing the a) heat transferred from the particles to the sCO$_2$ $\dot{Q}_f$ as a function of the excess dimensionless gas velocity $\widehat{U}$ and b) overall heat transfer coefficient U_{HX} with increasing excess dimensionless gas velocity $\widehat{U}$.

The discrepancy between model-predicted U_{HX} values derived from lab-scale tests and the measured values based on Eq. 2 may have arisen in large part from the axial dispersion of solid-particle thermal energy due to fluidization. Thermal energy dispersion was not included in the original reduced-order models [8]. During testing, the impact of dispersion was made evident by a significant difference between the particle inlet temperature $T_{s,in}$ from the feed hopper, and the measured freeboard zone temperature $T_{s,fb}$. The difference $T_{s,in} - T_{s,fb}$ was attributed to axial dispersion of particles due to fluidization bringing partially cooled particles from the fluidized channels back up into the freeboard zone to mix with the hot particles coming from the feed hopper. As shown in Fig. 3a), $T_{s,in} - T_{s,fb}$ increased with $\widehat{U}$ due to the increase in axial dispersion with increasing upward gas velocity but decreased with higher $\dot{m}_s$ since dispersion due to fluidization did not change with the net particle flow rate. The drop in freeboard zone temperature due to axial dispersion lowers the mean temperature difference between the particles and the counterflowing sCO$_2$ flows. This inherently reduces U_{HX} as defined by Eq. 2, which is based on a log mean temperature difference using $T_{s,in}$ even though heat transfer to the sCO$_2$ starts at $T_{s,fb}$. An alternative definition of the overall heat transfer coefficient $U_{HX,fb}$ based on $T_{s,fb}$ is given here in Eq. 3, and $U_{HX,fb}$ from the measured results is plotted in Fig. 3b).

$$\dot{Q}_f = U_{HX,fb} A_{w,tot} \Delta T_{lm,fb} = U_{HX} A_{w,tot} \frac{(T_{s,fb} - T_{sCO2,out}) - (T_{s,out} - T_{sCO2,in})}{\ln(T_{s,fb} - T_{sCO2,out}) - \ln(T_{s,out} - T_{sCO2,in})} \quad (3)$$

The modified $U_{HX,fb}$ does not represent the overall performance of the fluidized bed HX, but it does better represent how the heat transfer between the particles and the sCO$_2$ varies with $\widehat{U}$ over the full range of tested fluidizing gas flow conditions consistent with the trends observed in the lab-scale narrow-channel fluidized bed heat transfer studies [8]. This suggests that approaches to suppressing axial dispersion in the fluidized bed without suppressing particle-wall heat transfer will be critical for narrow-channel fluidized bed HX designs.

To further explore the impacts of axial dispersion, the reduced order model used in the design of a counterflow fluidized bed HX was updated to include the effects of axial solid particle dispersion due to fluidization. To this end, solid particle dispersion was added to the fluidized bed model which leads to an additional diffusive term the derivative of the vertical dispersion heat flux $\dot{q}''_{s,disp}$

in the solid phase thermal energy balance. The term shown here in Eq. 4 is modeled by a solid-phase vertical dispersion coefficient $D_{yy,s}$ that must be fitted to experimental measurements.

$$\frac{d\dot{q}''_{s,disp}}{dy} = \frac{d}{dy}\left(D_{yy,s}\phi_s\rho_s c_{p,s}\frac{dT_s}{dy}\right) \quad (4)$$

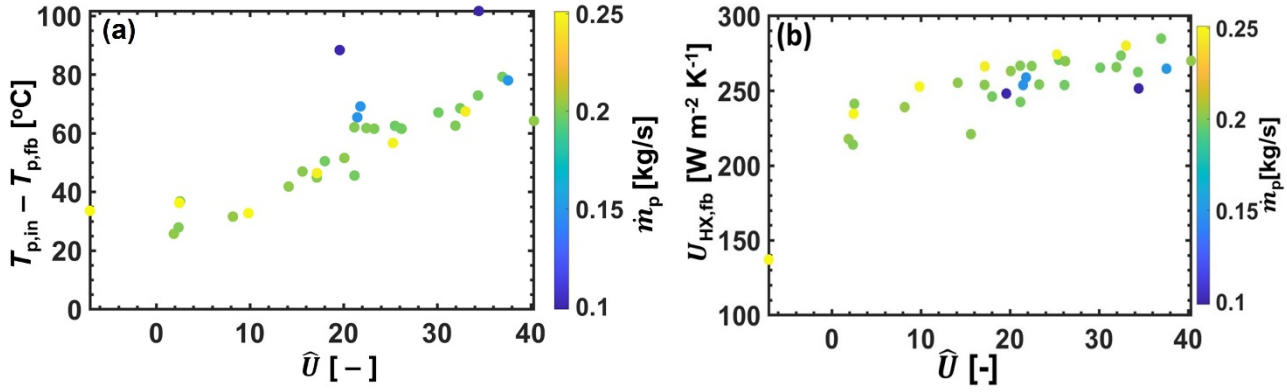

Figure 3. Experimental measurements of the particle flow rate $\dot{m}_s$ as colored points showing the a) temperature difference between the particles in the feed hopper (particle inlet, $T_{s,in}$) and the freeboard zone ($T_{s,fb}$) as a function of the excess dimensionless gas velocity $\hat{U}$ and b) modified overall heat transfer coefficient $U_{HX,fb}$ calculated using the freeboard zone particle temperature $T_{s,fb}$ with increasing excess dimensionless gas velocity $\hat{U}$.

Lab-scale testing in the single-channel test rig established that $D_{yy,s}$ is proportional to fluctuations in the product of solid volume fraction ϕ_s and pressure gradients dp/dy. Measurements of $D_{yy,s}$ in the lab-scale tests supporting this work are discussed more fully in a recent reference [10]. Previous studies of axial dispersion in fluidized beds have shown that $D_{yy,s}$ can be fit assuming a constant axial dispersion Peclet number $Pe_{y,s}$ as defined in Eq. 5 [11,12] where the hydraulic diameter equals $2\Delta x_b\Delta z_b/(\Delta z_b + \Delta z_b)$.

$$Pe_{y,s} = \frac{2\Delta z_b(u_g - u_{mf})}{D_{yy,s}} \quad (5)$$

From the single channel heat transfer test data with a similar bed geometry to the tested prototype HX, $Pe_{y,s}$ = 3.92 provided the best fit to the measurements of $D_{yy,s}$. From Eq. 5, $D_{yy,s}$ will increase linearly with excess fluidization velocity $u_g - u_{mf}$, which is consistent with the linear increase in $T_{s,in} - T_{s,fb}$ with $u_g - u_{mf}$ in the HX as shown in Fig. 3a. The updated counterflow fluidized bed HX reduced-order model that accounted for axial dispersion using Eq. 5, was run at the HX design conditions listed in Table 1 with CARBOBEAD HSP 45/60 particles to explore the impact of dispersion on the vertical HX temperature profiles and overall HX performance. Figure 4 compares the resulting temperature profiles for the sCO_2 microchannel flow, the fluidizing gas, solid particle flows, and HX walls for the cases with and without axial dispersion at $\dot{m}_s = \dot{m}_f$ =200 g s^{-1} and $\dot{m}_f$ =4 g s^{-1}. Without dispersion (Fig. 4a), the particle inlet temperature $T_{s,in}$ = $T_{s,fb}$ = 600 °C is sustained in the freeboard zone, which provides a ΔT_{lm}= 48.2 °C to support higher $\dot{Q}_f$ = 46.3 kW and higher U_{HX} = 500 W m^{-2} K^{-1} with an HX effectiveness ε_{HX} = 0.83. Adding in dispersion (Fig. 4b) leads to a significant $T_{s,in} - T_{s,fb}$ of approximately 40 °C reduces the driving force for transferring heat to the sCO_2 through the core walls. The presence of axial dispersion in the model results in a $\dot{Q}_f$ = 37.0 kW, U_{HX} = 243 W m^{-2} K^{-1} at ε_{HX} = 0.60, which is similar to the values recorded in the prototype HX. These modeling results support the conclusion that axial dispersion in the narrow channel fluidized bed can greatly impact the effectiveness of a fluidized bed particle-sCO_2

HX and designs that can suppress dispersion while maintaining the enhanced heat transfer will provide significant improvement in U_{HX} and thus a reduction in HX size and costs.

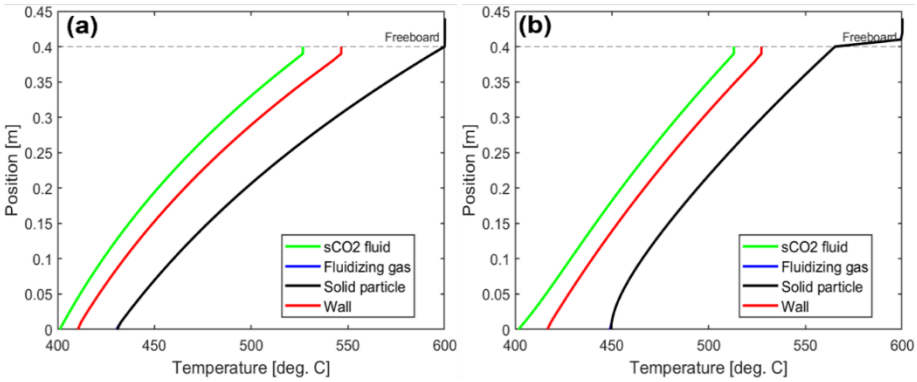

Figure 4. Temperature profiles of sCO_2, fluidizing gas, particles, and heat exchanger walls solved using a counterflow fluidized bed particle-sCO_2 heat exchanger reduced order model by Fosheim et al (2022) at the design conditions and listed in Table 1 for HX channels with 10.4 mm depth and 0.4 m high using CARBOBEAD HSP 45/60 particles where (a) axial dispersion is not accounted for resulting in a sCO_2 outlet temperature $T_{sCO2,out}$ =550 °C and an overall U_{HX} = 500 W m^{-2} K^{-1}, and (b) axial dispersion accounted for with a $Pe_{y,s}$ ≈3.92 resulting in a sCO_2 outlet temperature $T_{sCO2,out}$ ≈520 °C and an overall U_{HX} ≈ 243 W m^{-2} K^{-1}.

4. Conclusions

A nominal 40-kW_{th} prototype particle-sCO_2 HX was designed from a reduced-order model study and then fabricated and tested at Sandia's NSTTF for particle inlet temperatures over 500 °C. The initial reduced order model did not account for the effect of axial dispersion and predicted an overall heat transfer coefficient U_{HX} = 500 W m^{-2} K^{-1} for a shell-and-plate HX design with 12 parallel narrow-channel fluidized beds and microchannel sCO_2 flows embedded in the HX plate walls. The HX design included a common freeboard zone above the parallel channels which provided reliable particle flows and steady operation for overall heat transfer $\dot{Q}_f$ up to 40 kW. The tests, however, required higher particle mass flow rates than designed to achieve the desired $\dot{Q}_f$ because the overall U_{HX} never exceeded 205 W m^{-2} K^{-1}.

The tests revealed that despite improved particle-wall heat transfer with increasing fluidization velocities, $\dot{Q}_f$ reached a maximum at a very low excess fluidization velocity ($\widehat{U}$ ≈ 10) and remained nearly constant with further increases in gas velocity. This unexpected behavior was caused by increased axial dispersion with increased gas velocity in the fluidized bed lowering the temperature driving force in the HX due to vertical mixing and thereby offsetting improvements in particle-wall heat transfer. The reduced-order design models were upgraded to include this axial dispersion and showed predicted performance like that observed in the HX tests for the original design condition. The upgraded model predicts an overall U_{HX} = 243 W m^{-2} K^{-1} instead of 500 W m^{-2} K^{-1} at the design conditions of the HX.

Several design improvements can be made to improve the overall U_{HX} including implementing structures within the narrow-channel bed to disrupt axial dispersion. In addition, about 17% of the heat transfer area below the gas injectors operated as a moving packed bed, and designs with injectors beneath the core can improve overall U_{HX}. All the same, the HX tests demonstrate the ability for mild fluidization in parallel fluidized bed channels to provide reliable heat transfer in particle-sCO_2 HX. Analysis of the test results and reduced order modeling show that redesigning

a fluidized bed HX with reduced dispersion is a promising approach to reducing particle-sCO_2 HX size and hopefully cost for future CSP-TES applications.

Data availability statement

The data presented in this study is based on a proprietary design owned by Vacuum Process Engineering. Due to the confidential nature of the design, data is not publicly available, but for research purposes, interested parties can contact the corresponding author, Gregory S. Jackson.

Author Contributions

"Winfred J. Afrifa-Arthur-Arhin [Conceptualization of this study, Methodology, Software, Data curation, Writing- original draft preparation, editing], Jesse R. Fosheim [Conceptualization of this study, Methodology], Keaton J. Brewster [Data curation, writing - proofing], Kevin J. Albrecht [Methodology, Data curation], Dimitri A . Madden [Data curation], and Gregory S. Jackson [Data curation, conceptualization of this study, methodology, writing, principal author]."

Funding

This work has been supported by the US DOE Solar Energy Technology Office, under award #DE-EE0008538. The authors thank DOE program manager Shane Powers and former program manager Mark Lausten for their support in this work.

Competing interests

The authors declare no competing interests.

Funding

This work was performed under grants from the U.S. Department of Energy Solar Energy Technology Office under award numbers DE-EE0008538 and DE-EE0009812 (Shane Powers and Dr. Rajgopal Vijaykumar, program managers). The third author is supported by the National Science Foundation Graduate Research Fellowship under Grant No. DGE-2137099.

Acknowledgment

The authors acknowledge Mr. Dereje Amogne and Mr. Collin Johnson of VPE for their extensive help in fabricating and delivering the heat exchanger core for this study. The authors also acknowledge Mr. Anthony Evens at Sandia National Laboratory for his assistance in installing and instrumenting the heat exchanger at the NSTTF test facility. The authors also acknowledge Azariah Thompson, Katherine Schubert, and Dr. Wanjun Dang who assisted with the narrow-channel testing at the Colorado School of Mines HiTECs Lab.

References

[1] M. A. Reyes-Belmonte, E. Díaz, M. Romero, and J. González-Aguilar, "Particles-based thermal energy storage systems for concentrated solar power," AIP Conf. Proc., vol. 2033, 2018, doi: 10.1063/1.5067215.

[2] M. Mehos et al., "Concentrating Solar Power Gen3 Demonstration Roadmap," NrelTp-5500-67464, no. January, pp. 1–140, 2017, doi: 10.2172/1338899.

[3] C. S. Turchi, Z. Ma, T. W. Neises, and M. J. Wagner, "Thermodynamic study of advanced supercritical carbon dioxide power cycles for concentrating solar power systems," J. Sol. Energy Eng. Trans. ASME, vol. 135, no. 4, 2013, doi: 10.1115/1.4024030.

[4] K. J. Albrecht, H. F. Laubscher, C. P. Bowen, and C. K. Ho, “Performance Evaluation of a Prototype Moving Packed-Bed Particle / sCO 2 Heat Exchanger,” no. September 2022.

[5] J. R. Fosheim, X. Hernandez, W. J. Arthur-Arhin, C. P. Bowen, K. J. Albrecht, and G. S. Jackson, “Design of a 40-kWth Counterflow Particle-Supercritical Carbon Dioxide Narrow-Channel Fluidized Bed Heat Exchanger”.

[6] Arthur-Arhin, W., Fosheim, J. R., Brewster, K. J., Thompson, A., Albrecht, K. J., Amogne, D., & Jackson, G. S. (2022). Testing of a 40-kWth Counterflow Particle-Supercritical Carbon Dioxide Narrow-Channel, Fluidized Bed Heat Exchanger. In SolarPACES Conference Proceedings (Vol. 1).

[7] D. C. Miller, “Heat Transfer Characteristics of a Novel Fluidized Bed for Concentrating Solar with Thermal Energy Storage,” Colorado School of Mines, Golden, CO, 2017.

[8] J. R. Fosheim, X. Hernandez, J. Abraham, A. Thompson, B. Jesteadt, and G. S. Jackson, “Narrow-channel fluidized beds for particle-sCO2 heat exchangers in next generation CPS plants,” AIP Conf. Proc., vol. 2445, no. 1, p. 160007, May 2022, doi: 10.1063/5.0085934.

[9] O. Molerus, “Particle-to-gas heat transfer in particle beds at Peclet numbers Pe ≤ 10,” Powder Technol., vol. 90, no. 1, pp. 47–51, 1997, doi: 10.1016/S0032-5910(96)03197-X.

[10] K.J. Brewster, J. R. Fosheim, F. Municchi, W.J. Arthur-Arhin, G.S. Jackson, "Reduced-Order Modeling of Indirect Fluidized-Bed Particle Receivers with Axial Dispersion”, submitted for publication AIP Proceedings, presented at SolarPACES 2023.

[11] M.-S. Salehi, M. Askarishahi, and S. Radl, “Quantification of Solid Mixing in Bubbling Fluidized Beds via Two-Fluid Model Simulations,” Ind. Eng. Chem. Res., vol. 59, no. 22, pp. 10606–10621, 2020, doi: 10.1021/acs.iecr.9b06343.

[12] N. Mostoufi and J. Chaouki, “Local solid mixing in gas–solid fluidized beds,” Powder Technol., vol. 114, no. 1–3, pp. 23–31, Jan. 2001, doi: 10.1016/S0032-5910(00)00258-8.